Measurement Sensitivity Analysis of the Transient Hot Source Technique Applied to Flat and Cylindrical Samples

Jason Ostanek
Naval Surface Warfare Center,
Philadelphia Division,
5001 South Broad Street,
Philadelphia, PA 19112

Krishna Shah
Mechanical and Aerospace
Engineering Department,
The University of Texas at Arlington,
500 West First Street,
Arlington, TX 76019

Ankur Jain
Mechanical and Aerospace
Engineering Department,
The University of Texas at Arlington,
500 West First Street,
Arlington, TX 76019

The transient source measurement technique is a nonintrusive, nondestructive method of measuring the thermal properties of a given sample. The transient source technique has been implemented using a wide variety of sensor shapes or configurations. The modern transient plane source (TPS) sensor is a spiral-shaped sensor element which evolved from transient line and transient hot strip (THS) source techniques. Commercially available sensors employ a flat interface that works well when test samples have a smooth, flat surface. The present work provides the basis for a new, cylindrical strip (CS) sensor configuration to be applied to cylindrical surfaces. Specifically, this work uses parameter estimation theory to compare the performance of CS sensor configurations with a variety of existing flat sensor geometries, including TPS and THS. A single-parameter model for identifying thermal conductivity and a two-parameter model for identifying both thermal conductivity as well as volumetric heat capacity are considered. Results indicate that thermal property measurements may be carried out with greater measurement sensitivity using the CS sensor configuration than similar configurations for flat geometries. In addition, this paper shows how the CS sensor may be modified to adjust the characteristic time scale of the experiment, if needed. [DOI: 10.1115/1.4034178]

Keywords: thermal property measurement, transient source techniques, parameter estimation, sensitivity analysis, thermal modeling

Introduction

The transient source method is a nonintrusive, nondestructive technique for measurement of thermal transport properties of a material [1–6]. The method is based on application of a known heating rate to the surface of a sample and measurement of the resulting temperature response at that surface. The heat source is typically a thin metallic foil having a nonzero temperature coefficient of resistivity, such as nickel or platinum. Heat is generated by supplying constant electrical current to the sensor. As the temperature of the sensor increases, the electrical resistance of the sensor increases proportionally. Since current is held constant, the voltage across the sensor is proportional to its temperature, via Ohm's law. This voltage is recorded as a function of time and compared with an appropriate model in order to identify the thermal parameter(s) of the given material.

The transient source method is based on the work of numerous researchers. The work by Gustafsson et al. [1–4] formed the basis for the modern TPS sensor. The concept originated with the THS sensor [2], which was essentially a long, thin sensor placed at the interface between two identical samples. Advancements to the original sensor resulted in the integration of an insulated backing such that the sensor and backing formed a "probe" [3]. Additionally, advancements in the shape of the sensor resulted in a bifilar spiral pattern rather than a flat strip [4]. Mathis took a similar approach, starting with a strip sensor [5]. However, one key difference is that Mathis installed guard heater strips on either side of the main sensing element to enforce one-dimensional heat flow normal to the measurement plane. This guarded hot strip design will be referred to here as the guarded transient hot strip (GTHS) sensor. Similar to the THS probe, the original GTHS design evolved into a bifilar spiral with a guard ring surrounding the main sensing element [6]. This approach is referred to as the guarded TPS sensor (GTPS). The GTHS and GTPS approaches simplify the analytical model relative to the THS/TPS probes due to the one-dimensional nature of heat flow. However, the nature of heat flow in the GTHS/GTPS probes prohibits the simultaneous identification of two thermal parameters (thermal diffusivity and thermal conductivity, for example). The TPS sensor, on the other hand, can identify two thermal parameters from a single transient recording.

With the wide variety in sensor configurations, the question of optimality becomes important in order to select the best sensor configuration for a given problem or a given material. Bohac et al. [7] applied parameter estimation theory to the TPS sensor with the goal of identifying the optimal experiment duration which maximizes measurement sensitivity. However, to the best of our knowledge, there has been no overall comparison of the various sensor configurations with regard to measurement sensitivity. This paper applies the principles of parameter estimation theory to several existing sensors (THS, TPS, GTHS, and GTPS) as well as to several new sensors appropriate for cylindrical geometries. The sensitivity of each sensor is compared for identifying thermal conductivity, λ, in a single-parameter model. Similarly, a two-parameter model is considered for identifying volumetric heat capacity, $\rho \cdot C_p$, in addition to thermal conductivity, λ. The results illustrate the advantages of certain sensor configurations and provide the theoretical basis for a new class of sensors aimed at measuring thermal properties from cylindrical surfaces.

In the Sensor Configurations section, several sensor geometries are described along with their corresponding mathematical models and analytical solutions. Model verification is then performed by comparing analytical solutions with numerical solutions. Following model verification, parameter estimation theory is discussed for a single-parameter model to identify thermal conductivity as well as a two-parameter model to identify thermal conductivity

Contributed by the Heat Transfer Division of ASME for publication in the JOURNAL OF THERMAL SCIENCE AND ENGINEERING APPLICATIONS. Manuscript received January 26, 2016; final manuscript received June 15, 2016; published online September 8, 2016. Assoc. Editor: Steve Q. Cai.

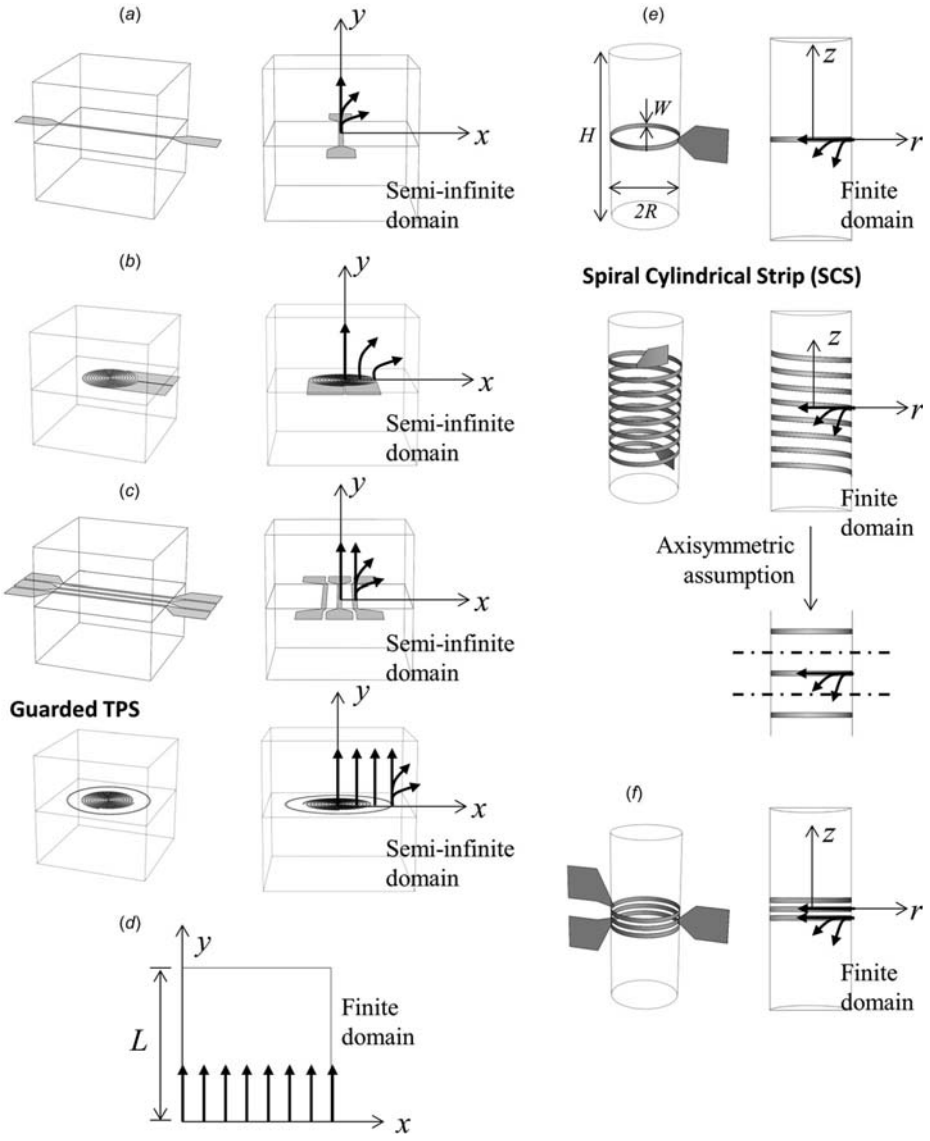

Fig. 1 Sketches of various transient heat source sensors. CS, GCS, and SCS sensor configurations are unique to the present work. Also shown are the coordinate system definitions and representative heat flow vectors depicting the mathematical model to be used for each sensor. (*a*) Transient hot strip (THS), (*b*) transient plane source (TPS), (*c*) guarded THS, (*d*) 1D finite slab, (*e*) cylindrical strip (CS), and (*f*) guarded CS.

and volumetric heat capacity. The results and discussion include a comparison of all the sensor configurations, flat and cylindrical, as well as a detailed analysis of the cylindrical configurations. Finally, the concluding section summarizes the work and discusses implications of the results.

Sensor Configurations

In this analysis, seven sensor configurations were considered as shown in Fig. 1. Figure 1(*a*) shows the THS method developed by Gustafsson et al. [2], where heat flow from the sensor is two-dimensional in the x–y plane. The sensor length is typically much greater than its width or thickness; therefore, heat transfer in the z-direction may be neglected. The TPS sensor, developed by Gustafsson et al. [4], is shown in Fig. 1(*b*). In this case, heat flow is three-dimensional in Cartesian coordinates. Or, using symmetry about the sensor axis, heat flow is two-dimensional in the r–z plane in cylindrical coordinates. Figure 1(*c*) shows two sensors, the GTHS, developed by Mathis [5], and the GTPS sensor, described in the patent of Emmanuel et al. [6]. These two sensor configurations are both shown in Fig. 1(*c*) because the mathematical model describing their heat flow is identical, as will be discussed shortly. For the GTHS and GTPS, guard heaters are used to enforce one-dimensional flow in the y-direction. The GTHS sensor uses two guard heater strips on either side of the main sensor, and the GTPS sensor uses a guard heater ring surrounding the main, spiral-shaped sensor. Figure 1(*d*) shows a one-dimensional, finite slab. As with the GTHS/GTPS configurations, heat flow is one-dimensional in the y-direction. The primary difference between the slab and the GTHS/GTPS configurations is that the slab domain is finite, having length L, as indicated in the figure. The THS, TPS, GTHS, and GTPS configurations assume a semi-infinite medium, as indicated in the figures.

Figures 1(*e*) and 1(*f*) show three additional heating/sensing configurations particularly appropriate for cylindrical geometries that have not been investigated in prior work. Figure 1(*e*) shows the CS and spiral cylindrical strip (SCS) configurations. As with the

GTHS/GTPS sensors, the CS and SCS sensors are both shown in Fig. 1(*e*) because the mathematical model is identical for the two configurations. In both CS and SCS sensors, heat flow is assumed to be axisymmetric, and thus two-dimensional in the *r*–*z* plane. The axisymmetric assumption has the implication that the SCS sensor neglects the pitch of the helical coil and, instead, may be represented by a series of parallel CS strips, as indicated in Fig. 1(*e*). Figure 1(*f*) shows the guarded cylindrical strip method (GCS), which features guard strips to ensure one-dimensional heat flow in the *r*-direction. Note that this setup is analogous to enforcing a constant heat flux across the entire outer radius of the cylinder, by wrapping a flat surface heater around the cylinder, for example. This approach was taken by Drake et al. [8] to investigate thermal properties of lithium-ion batteries.

The mathematical models for data analysis and thermal property extraction for each sensor configuration are summarized in Table 1. The models in Table 1 are labeled (*a*)–(*f*) corresponding to the sensor configurations shown in Fig. 1. Table 1 includes the governing heat conduction equations, simplified from their full three-dimensional formulations according to the listed assumptions. The full, three-dimensional heat conduction equation for Cartesian coordinate systems is

$$\rho C_p \frac{\partial \theta}{\partial t} = \lambda_x \frac{\partial^2 \theta}{\partial x^2} + \lambda_y \frac{\partial^2 \theta}{\partial y^2} + \lambda_z \frac{\partial^2 \theta}{\partial z^2} \tag{1}$$

The dependent variable in Eq. (1) is temperature rise of the sensor, $\theta(t) = T(t) - T_0$. In Eq. (1), it is assumed that thermal conductivity does not vary with temperature and it is assumed that the temperature everywhere in the domain is T_0 at $t = 0$. Similarly, for cylindrical coordinates

$$\rho C_p \frac{\partial \theta}{\partial t} = \frac{\lambda_r}{r} \frac{\partial}{\partial r}\left(r \frac{\partial \theta}{\partial r}\right) + \frac{\lambda_\phi}{r^2} \frac{\partial^2 \theta}{\partial \phi^2} + \lambda_z \frac{\partial^2 \theta}{\partial z^2} \tag{2}$$

Table 1 Summary of sensor configurations and corresponding mathematical models

Description	Simplified governing equation	Boundary and initial conditions	Assumptions
(a) THS	$\frac{1}{\kappa}\frac{\partial \theta}{\partial t} = \frac{\partial^2 \theta}{\partial x^2} + \frac{\partial^2 \theta}{\partial y^2}$	$\theta(t,x,y,z) \to 0$ as $x,y,z \to \infty$ $\frac{\partial \theta(t,x,0,z)}{\partial y} = \begin{cases} -\frac{q''}{\lambda} & \text{for heated area} \\ 0 & \text{otherwise} \end{cases}$ $\frac{\partial \theta(t,0,y,z)}{\partial x} = 0, \frac{\partial \theta(t,x,y,0)}{\partial z} = 0$ $\theta(0,x,y,z) = 0$	Homogeneous and isotropic medium Semi-infinite medium: $x = (-\infty,\infty)$, $y = [0,\infty)$, $z = (-\infty,\infty)$ Symmetry about $x = 0$ and $z = 0$ At $y = 0$, constant heat flux in heated areas and perfect insulation in nonheated areas No heat flow in z-direction
(b) TPS	$\frac{1}{\kappa}\frac{\partial \theta}{\partial t} = \frac{\partial^2 \theta}{\partial x^2} + \frac{\partial^2 \theta}{\partial y^2} + \frac{\partial^2 \theta}{\partial z^2}$	$\theta(t,x,y,z) \to 0$ as $x,y,z \to \infty$ $\frac{\partial \theta(t,x,0,z)}{\partial y} = \begin{cases} -\frac{q''}{\lambda} & \text{for heated area} \\ 0 & \text{otherwise} \end{cases}$ $\frac{\partial \theta(t,0,y,z)}{\partial x} = 0, \frac{\partial \theta(t,x,y,0)}{\partial z} = 0$ $\theta(0,x,y,z) = 0$	Homogeneous and isotropic medium Semi-infinite medium: $x = (-\infty,\infty)$, $y = [0,\infty)$, $z = (-\infty,\infty)$ Symmetry about $x = 0$ and $z = 0$ At $y = 0$, constant heat flux in heated areas and perfect insulation in nonheated areas
(c) GTHS, GTPS	$\frac{1}{\kappa}\frac{\partial \theta}{\partial t} = \frac{\partial^2 \theta}{\partial y^2}$	$\theta(t,y) \to 0$ *as* $y \to \infty$ $\frac{\partial \theta(t,0)}{\partial y} = -\frac{q''}{\lambda}$ $\theta(0,y) = 0$	Homogeneous and isotropic medium Semi-infinite medium: $x = (-\infty,\infty)$, $y = [0,\infty)$, $z = (-\infty,\infty)$ Constant heat flux at $y = 0$ One-dimensional heat flow
(d) One-dimensional finite slab	$\frac{1}{\kappa}\frac{\partial \theta}{\partial t} = \frac{\partial^2 \theta}{\partial y^2}$	$\frac{\partial \theta(t,0)}{\partial y} = -\frac{q''}{\lambda}$ $\frac{\partial \theta(t,L)}{\partial y} = 0$ $\theta(0,y) = 0$	Homogeneous and isotropic medium Constant heat flux at $y = 0$ One-dimensional heat flow
(e) CS, SCS	$\frac{1}{\kappa}\frac{\partial \theta}{\partial t} = \frac{1}{r}\frac{\partial}{\partial r}\left(r\frac{\partial \theta}{\partial r}\right) + \frac{\partial^2 \theta}{\partial z^2}$	$\frac{\partial \theta(t,0,z)}{\partial r} = 0$ $\frac{\partial \theta(t,R,z)}{\partial r} = \begin{cases} \frac{q''}{\lambda} & \text{for heated area} \\ 0 & \text{otherwise} \end{cases}$ $\frac{\partial \theta(t,r,-H/2)}{\partial z} = 0, \frac{\partial \theta(t,r,H/2)}{\partial z} = 0$ $\theta(0,r,z) = 0$	Homogeneous and isotropic medium At $r = R$, constant heat flux in heated area and perfect insulation in nonheated areas Symmetry about $r = 0$ No heat flow in ϕ-direction Perfect insulation at $z = -H/2$ and $H/2$
(f) GCS	$\frac{1}{\kappa}\frac{\partial \theta}{\partial t} = \frac{1}{r}\frac{\partial}{\partial r}\left(r\frac{\partial \theta}{\partial r}\right)$	$\frac{\partial \theta(t,0,z)}{\partial r} = 0$ $\frac{\partial \theta(t,R,z)}{\partial r} = \frac{q''}{\lambda}$ $\theta(0,r) = 0$	Homogeneous and isotropic medium Constant heat flux at $r = R$ Symmetry about $r = 0$ One-dimensional heat flow

Table 2 Analytical solutions for average sensor temperature rise versus time

Sensor	Solution method	Analytical solution(s)	Reference
(a) THS	Green's function theory	$\bar{\theta}(\tau)=\frac{q''\tau}{4W\lambda\sqrt{\pi}}\left\{1-\text{erfc}(\tau^{-1})-\frac{\tau\left[1-\exp(-\tau^{-2})\right]}{2\sqrt{\pi}}-\frac{\text{Ei}(-\tau^{-2})}{2\tau\sqrt{\pi}}\right\}$ $\tau=\frac{\sqrt{\kappa t}}{(0.5W)}$ where W is the width of the sensor	Gustafsson et al. [2]
(b) TPS	Green's function theory	$\bar{\theta}(\tau)=\frac{q''R}{2\lambda}\int_0^R \pi r dr\int_0^\infty \frac{d\lambda'}{\lambda'}J_0(\lambda' r)J_1(\lambda' a)\left[erfc(-\lambda' R\tau)-erfc(\lambda' R\tau)\right]$ $\tau=\frac{\sqrt{\kappa t}}{R}$ where R is the sensor radius	Shown here, sensor is approximated as a disk source. Carslaw and Jaeger [9], p. 264 Gustafsson et al. [4] derived the solution for a series of concentric ring sources
(c) GTHS, GTPS	Green's function theory	$\bar{\theta}(\tau)=\frac{q''L\tau}{\lambda\sqrt{\pi}}$ $\tau=\frac{\sqrt{\kappa t}}{L}$ where L is the unit length, 1 m	Carslaw and Jaeger [9], p. 75
(d) One-dimensional finite slab	Separation of variables	$\bar{\theta}(\tau)=\frac{2q''L\tau}{\lambda}\sum_{n=0}^{\infty}\left\{\text{ierfc}\frac{n}{\tau}+\text{ierfc}\frac{(n+1)}{\tau}\right\}$ $\tau=\frac{\sqrt{\kappa t}}{L}$ where L is the thickness of the slab	Carslaw and Jaeger [9], p. 112
(e) CS, SCS	Laplace transform	$\bar{\bar{\theta}}(s)=c_0 I_0(\mu_0 r)+\frac{\sum_{n=1}^{\infty}\frac{c_n H\cdot I_0(\mu_n r)}{n\pi}\left[\sin\left(\frac{n\pi(H+W)}{2H}\right)-\sin\left(\frac{n\pi(H-W)}{2H}\right)\right]}{W}$ $\mu_n=\sqrt{\left[\left(\frac{n\pi}{2H}\right)^2+\frac{s}{\kappa}\right]};\ c_0=\frac{q''\cdot W}{s\lambda\mu_0 H\cdot I_1(\mu_0 R)}\ c_n=\frac{2\cdot q''\left[\sin\left(\frac{n\pi\cdot(H+W)}{2H}\right)-\sin\left(\frac{n\pi\cdot(H-W)}{2H}\right)\right]}{n\pi\cdot s\lambda\mu_n I_1(\mu_n R)}$ where H is the length of the cylinder, R is the radius, and W is the width of the sensor	Present work
(f) GCS	Separation of variables	$\bar{\theta}(\tau)=-\frac{q''R}{\lambda}\left[2\tau^2+\frac{1}{4}-2\sum_{s=1}^{\infty}e^{-a_s^2\tau^2}\cdot\frac{J_0(a_s)}{a_s^2 J_0(a_s)}\right]$ $\tau=\frac{\sqrt{\kappa t}}{R}$ where a_s are the positive roots of $J_1(a)=0$, and R is the sample radius	Carslaw and Jaeger [9], pp. 328–329

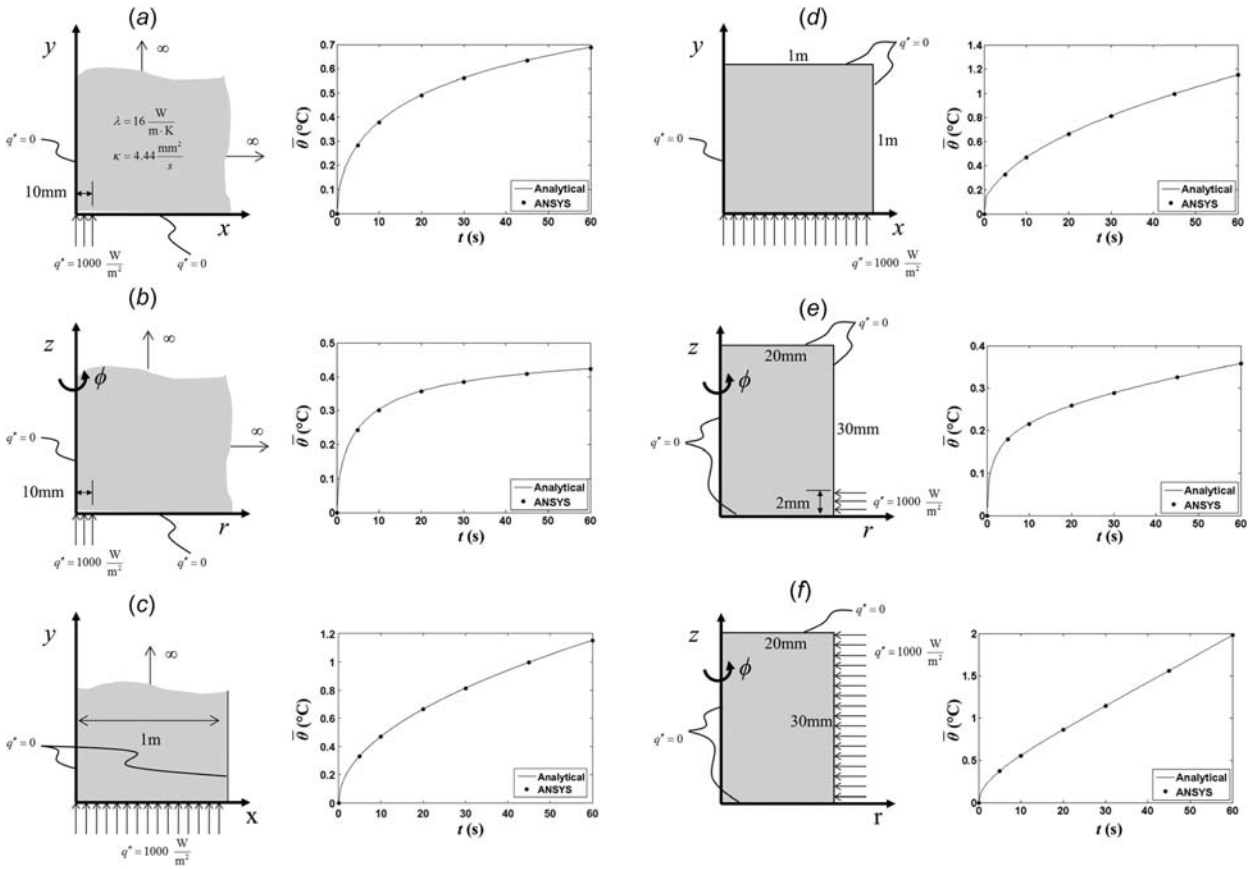

Fig. 2 Schematic drawings (not to scale) of solution domain and boundary conditions and verification data comparing analytical solutions (lines) with numerical solutions (symbols). The analytical solutions used for each sensor configuration are indicated in Table 2. (*a*) THS, (*b*) TPS, (*c*) GTHS, GTPS, (*d*) 1D finite slab, (*e*) CS, SCS, and (*f*) GCS.

Boundary and initial conditions are also shown in Table 1, in accordance with the list of assumptions for each sensor configuration.

The solution methods and the corresponding analytical solutions for each model are shown in Table 2. As with Table 1, the solutions in Table 2 are labeled (*a*)–(*f*) corresponding to the sensor configurations shown in Fig. 1. Most of the analytical solutions are available in Carslaw and Jaeger [9]. Note that the analytical solutions in Table 2 are written for the spatially averaged sensor temperature as a function of time, denoted with an overbar on the temperature variable. Also, note that the average sensor temperature varies as a function of τ, which is a nondimensional time scale proportional to the square root of time. The one exception is the CS sensor model, which was solved using Laplace transform, and the average sensor temperature given in Table 2 is presented in the transform domain, where the independent variable is s and the dependent variable is the Laplace-transformed average sensor temperature, denoted by a double-overbar. An inverse Laplace transform is performed numerically using well-established numerical algorithms [10] to obtain the time-domain solution, which can then be tabulated as a function of τ.

Model Verification

The analytical solution for each sensor design was verified by comparison with numerical solution. Numerical solutions were obtained using ANSYS™ MECHANICAL APDL finite-element analysis (FEA) software. A schematic of each model is shown in Fig. 2. For each case, the material properties were assigned to represent stainless steel. Thermal conductivity and thermal diffusivity were, $\lambda = 16\,\text{W/(m K)}$ and $\kappa = 4.44\ \text{mm}^2/\text{s}$, respectively. The numerical and analytical solutions were carried out to 60 s, and the numerical solution was advanced in time steps of 0.5 s. A constant heat flux of $q'' = 1000\,\text{W/m}^2$ was applied to the sensor area. Quadratic elements, which use midside nodes, were used in favor of linear elements for improved convergence properties.

Several of the analytical models considered here assume that heat is dissipated into an infinite medium (TPS, THS, GTPS, and GTHS). In order to numerically model a domain of infinite extent, the domain boundaries were set very far from the heat source, and the solution duration was set to less than 0.1% of the approximate diffusive time scale for heat to travel from the heat source to the nearest boundary.

The resulting comparisons between numerical and analytical solutions for each geometric configuration are shown in Fig. 2. The verification plots in Fig. 2 are labeled (*a*)–(*f*) corresponding to the sensor configurations in Fig. 1. As expected, good agreement was observed between the two solution methods in each case. Therefore, the analytical solutions were verified to be derived and programed correctly.

Single-Parameter ($p = 1$), Nonlinear Model

The following analysis is based on the work of Beck and Arnold [11] and uses parameter estimation theory to quantify measurement sensitivity for a variety of transient source sensor configurations. The sensor configurations investigated here are summarized in Table 2 along with their corresponding analytical solutions.

For the sensitivity analysis, the same material properties were used as for the model verification study ($\lambda = 16\,\text{W/(m K)}$ and $\kappa = 4.44\ \text{mm}^2/\text{s}$). Similarly, the same heat flux was applied to the sensor area ($q'' = 1000\,\text{W/m}^2$). The results are presented

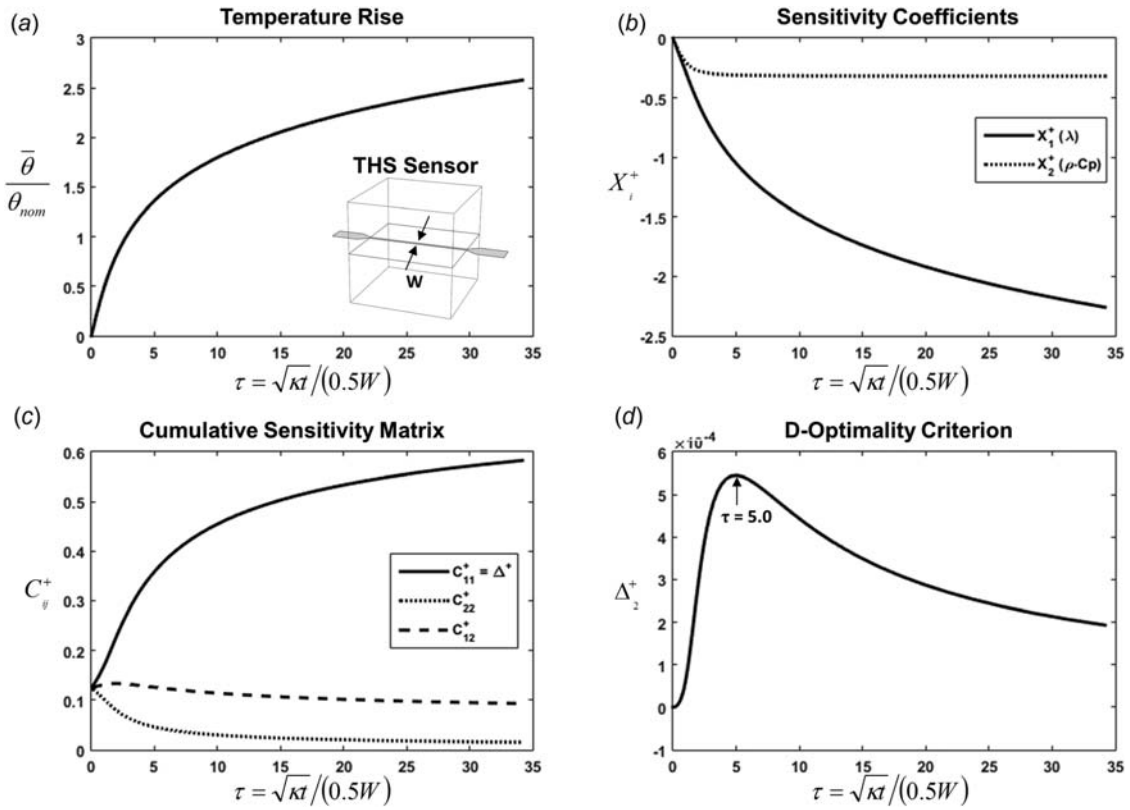

Fig. 3 Measurement sensitivity analysis for THS geometry: temperature rise (*a*), sensitivity coefficients (*b*), covariance matrix components (*c*), and D-optimality criteria (*d*)

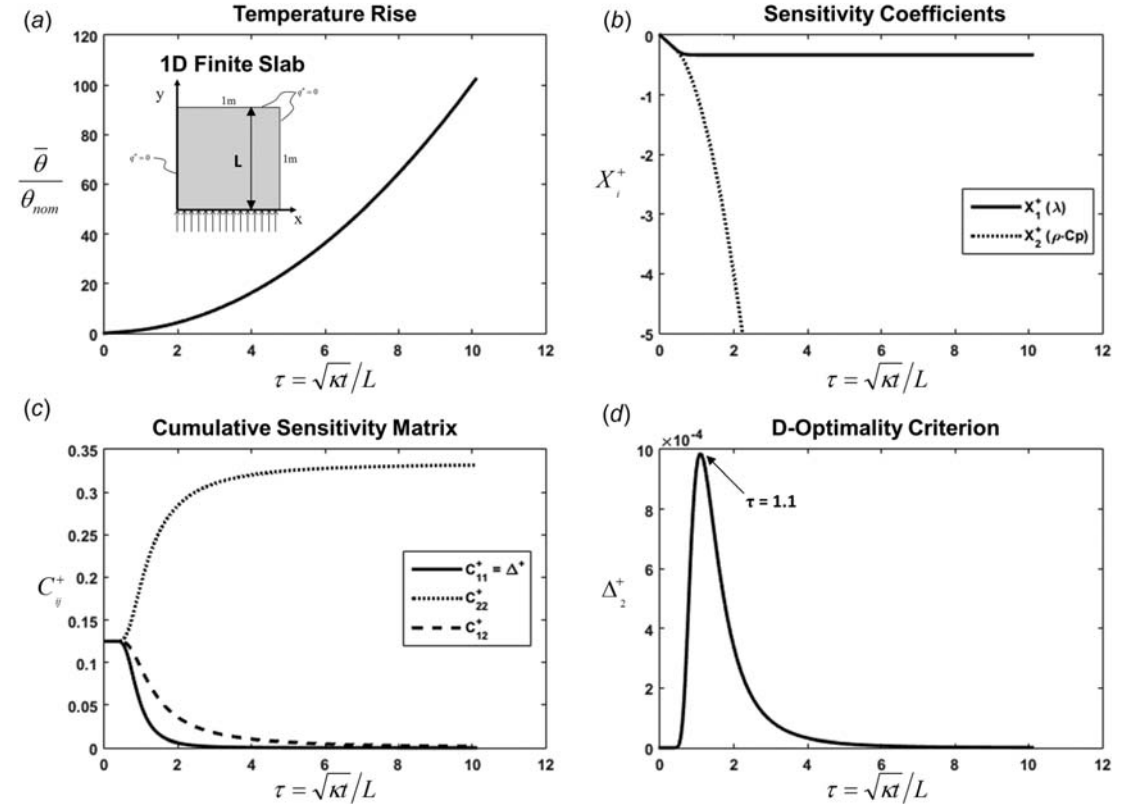

Fig. 4 Measurement sensitivity analysis for a 1D finite slab: temperature rise (*a*), sensitivity coefficients (*b*), covariance matrix components (*c*), and D-optimality criteria (*d*)

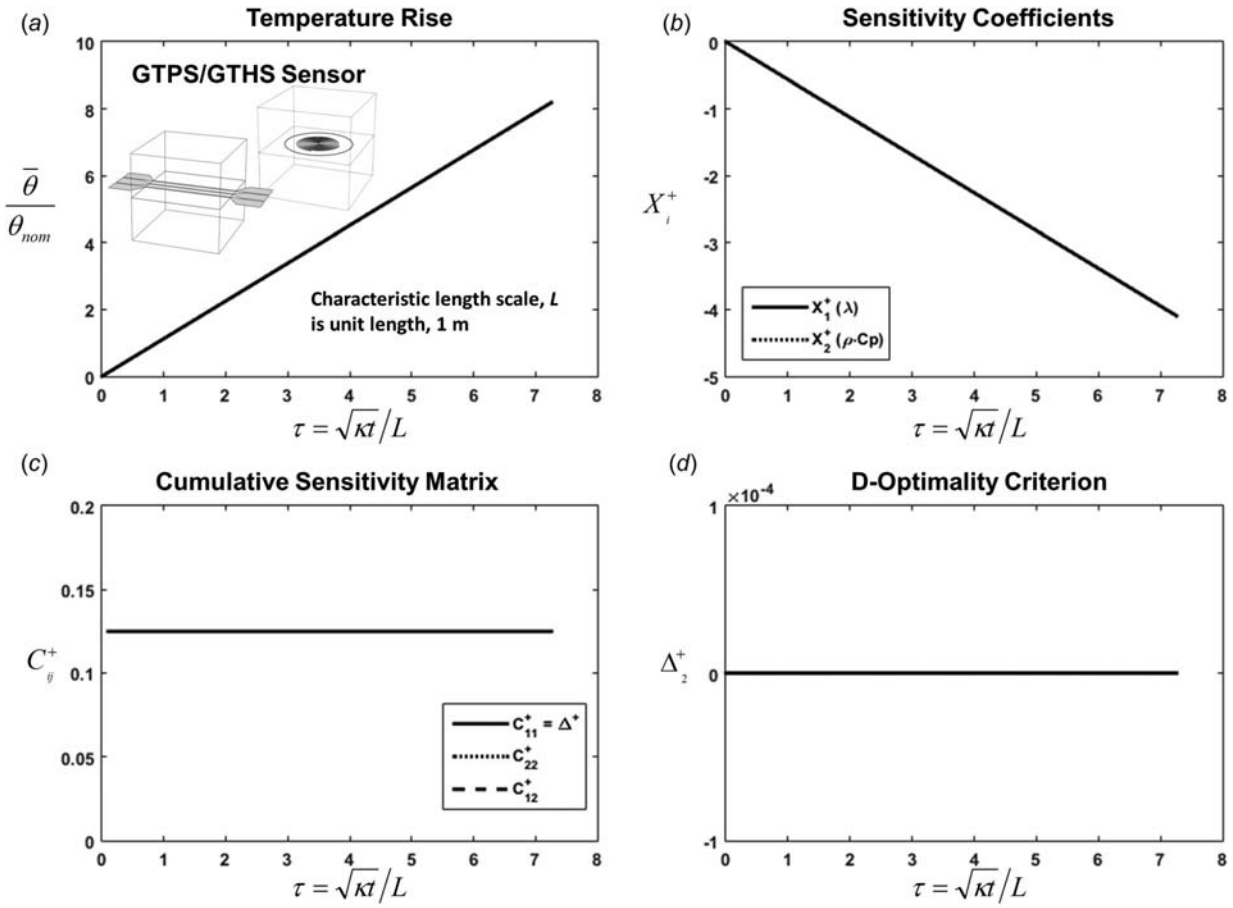

Fig. 5 Measurement sensitivity analysis for GTPS/GTHS configuration: temperature rise (*a*), sensitivity coefficients (*b*), covariance matrix components (*c*), and D-optimality criteria (*d*)

nondimensionally, however, such that they can be applied in a general sense. In this analysis, the time duration was extended beyond 60 s, to ensure that all the salient features relevant to the sensitivity analysis were captured.

The expression for estimated parameter variance depends on several assumptions regarding measurement errors. It is assumed that measurement errors are additive, have zero-mean, have constant variance, are uncorrelated, and have normal distribution. Additional assumptions include errorless independent variables and no prior information regarding the parameters of interest other than that they are nonrandom. With these assumptions, the variance of the estimated parameter, b, is

$$V(b) \cong \frac{\sigma^2}{\Delta^+} \tag{3}$$

$$\Delta^+ = \frac{1}{\tau}\int_0^\tau \left(X^+\right)^2 \left(\theta_m^+\right)^{-2} d\tau' \tag{4}$$

$$X^+ = \frac{\beta}{\theta_{\text{nom}}}\frac{\partial \bar{\theta}}{\partial \beta} \tag{5}$$

$$\theta_m^+ = \frac{\bar{\theta}(\tau)}{\theta_{\text{nom}}} \tag{6}$$

$$\theta_{\text{nom}} = \left(\frac{q''L}{\lambda}\right) \tag{7}$$

In Eq. (3), Δ^+ is the D-optimality criterion, and σ^2 is the variance of the observation errors. In Eq. (4), τ is the experiment duration, X^+ is the nondimensional sensitivity coefficient, and θ_m^+ is the maximum temperature rise. In Eq. (5), β is the parameter of interest, and θ_{nom} is the nominal temperature rise. From Eq. (6), note that θ_m^+ is a function of τ, the limit of integration in Eq. (2), and not the integration variable, τ'. And, from Eq. (7), L is a characteristic length scale.

As discussed by Beck and Arnold [11], Eq. (4) provides the optimality criterion for a single-parameter, nonlinear model. Maximizing Δ^+ will minimize the variance in the estimated parameter. The optimal duration of the experiment would be the time, τ, at which Δ^+ is a maximum.

Two-Parameter ($p = 2$), Nonlinear Model

For the single-parameter model, Eq. (3) shows that minimizing the variance of the estimated parameter is accomplished through maximizing Δ^+, see Eq. (4). The same principle is true for the two-parameter model, with the exception that the criterion is to maximize the determinant of the cumulative sensitivity coefficient matrix, $\mathbf{C}_{ij}^+$

$$\mathbf{C}_{ij}^+ = \frac{1}{\tau}\int_0^\tau \mathbf{X}_i^+ X_j^+ \left(\theta_m^+\right)^{-2} d\tau' \tag{8}$$

where $i = 1$ to p and $j = 1$ to p. For the two-parameter model, the determinant of the $\mathbf{C}_{ij}^+$ matrix of order two is readily calculated

$$\Delta_2^+ = C_{11}^+ C_{22}^+ - \left(C_{12}^+\right)^2 \tag{9}$$

Note that Eq. (8) is identical to Eq. (4) when $i = j$. In other words, the terms on the primary diagonal of the C_{ij}^+ matrix are equivalent

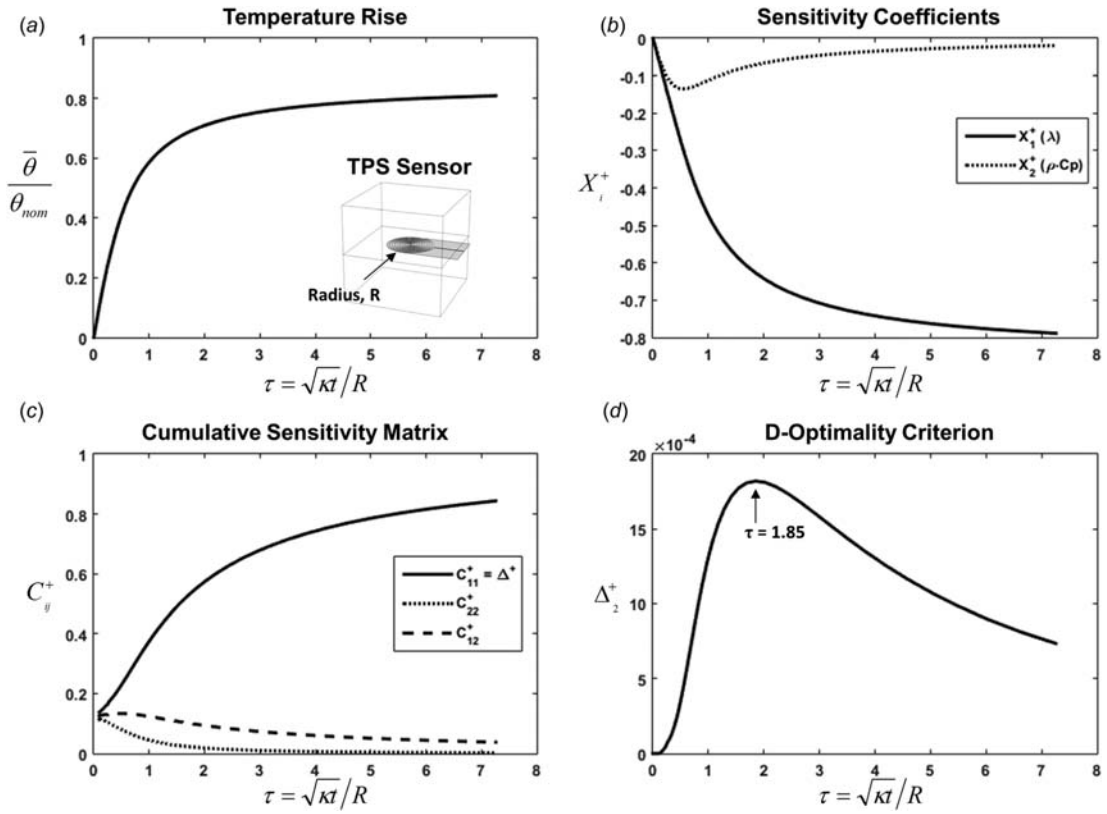

Fig. 6 Measurement sensitivity analysis for TPS geometry: temperature rise (*a*), sensitivity coefficients (*b*), covariance matrix components (*c*), and D-optimality criteria (*d*)

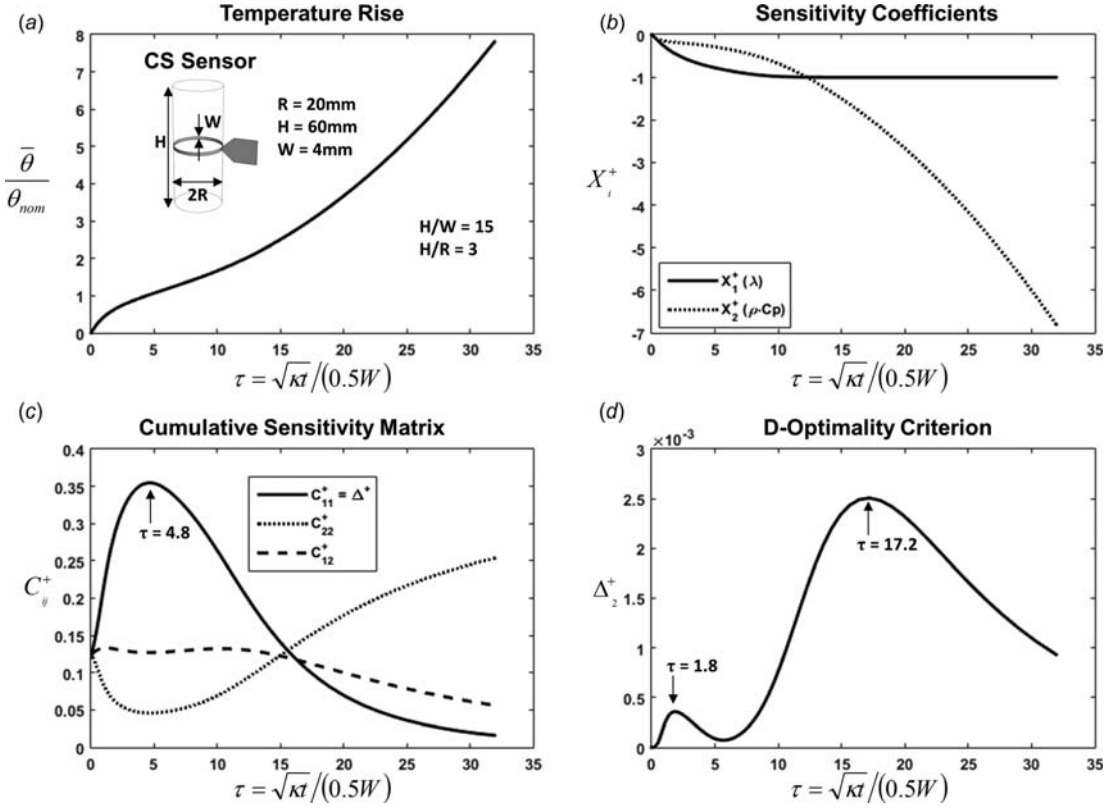

Fig. 7 Measurement sensitivity analysis for CS geometry: temperature rise (*a*), sensitivity coefficients (*b*), covariance matrix components (*c*), and D-optimality criteria (*d*)

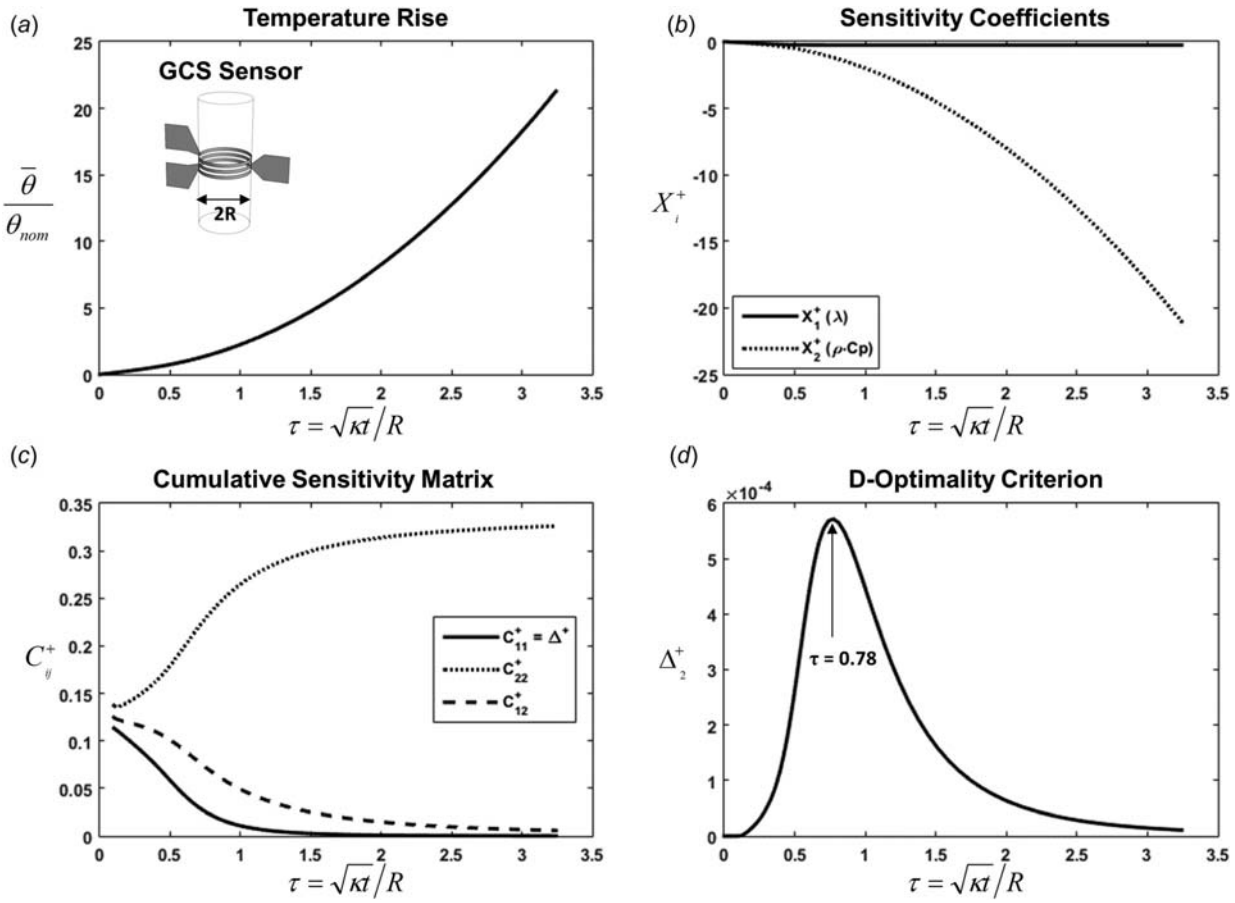

Fig. 8 Measurement sensitivity analysis for GCS geometry: temperature rise (*a*), sensitivity coefficients (*b*), covariance matrix components (*c*), and D-optimality criteria (*d*)

to the single-parameter D-optimality criterion for the p parameters.

Comparison of Sensor Configurations

In this section, results are presented for each sensor configuration in order to draw comparisons between various sensor shapes. Figures 3–8 show the results of the sensitivity analysis for each sensor. In each figure, the nondimensional temperature rise is shown in (*a*), the sensitivity coefficients are shown in (*b*), the cumulative sensitivity matrix components are shown in (*c*), and the D-optimality criterion for the two-parameter model, Δ_2^+, is shown in (*d*). The optimization criterion for estimating thermal conductivity using the single-parameter model is shown in (*c*) of each figure where $C_{11}^+ = \Delta^+$.

The results for the THS sensor are shown in Fig. 3. Note that the characteristic length scale used in the definition of τ was the sensor half-width, $W/2$. When estimating the thermal conductivity using a single-parameter model, the optimization criterion is Δ^+ is shown in Fig. 3(*c*). From Fig. 3(*c*), Δ^+ is found to continually increase with time. Theoretically, the experiment would be carried out as long as possible to obtain an increasingly improved estimate of λ. It is not practical, however, to carry out the experiment for very long times because heat will eventually reach the boundary of the test sample and violate the semi-infinite assumptions of the mathematical model. For the purpose of comparison with other sensors, the limiting value was estimated to be $\Delta^+ \to 0.86$ as $\tau \to \infty$ (although not shown in Fig. 3(*c*)). For the two-parameter model, the optimization criterion is obtained from Fig. 3(*d*). In this case, a maximum Δ_2^+ of 5.5×10^{-4} occurred at $\tau = 5.0$ indicating the optimal experiment duration for identifying the two parameters, λ and $\rho \cdot C_p$.

The results for the TPS sensor are shown in Fig. 4. The characteristic length scale is the sensor radius, R. Similar to the THS sensor, Fig. 4(*c*) shows that the optimization criterion for the single-parameter model, C_{11}^+, increases continually. As time approaches infinity, Δ^+ approaches 1.0 (not pictured). For the two-parameter model, Fig. 4(*d*) shows a maximum Δ_2^+ of 1.8×10^{-3} occurring at $\tau = 1.85$. In comparison to the THS sensor, the TPS sensor will have lower variance in estimated thermal conductivity (better performance) when using the single-parameter model. Similarly, the finite slab will have improved sensitivity when identifying two parameters since the maximum value of Δ_2^+ is higher for the TPS sensor than for the THS sensor.

The GTPS and GTHS sensors each use the same model and analytical solution. Figure 5, therefore, represents data for both sensor configurations. Because the problem is set up as one-dimensional heat flow in a semi-infinite domain, there is no characteristic length scale. To preserve the dimensionless parameter, τ, unit length was used for the characteristic length scale. The sensitivity coefficients shown in Fig. 5(*b*) are linearly dependent and are, in fact, identical. As a result, the two-parameter model is not applicable since there is no way to distinguish whether changes in temperature are caused by changes in thermal conductivity or volumetric heat capacity. As such, $\Delta_2^+ = 0$ for all times, as shown in Fig. 5(*d*). Thus, the GTPS sensor [2–4,8] can only identify one parameter at a time or a combination of the two parameters. The optimization criterion for the single-parameter model, shown in Fig. 5(*c*), is $\Delta^+ = 0.125$ at all times. Continuing the experiment will provide no greater advantage from the standpoint of the Δ^+ optimization criterion. Experiment duration may be selected based

Table 3 Comparison of sensor geometry showing sensitivity to thermal conductivity (single-parameter model) and sensitivity to conductivity and volumetric heat capacity (two-parameter model)

Sensor	Length scale	Dimensionless time scale	Single-parameter model (λ)	Two-parameter model (λ and ρC_p)
THS	Sensor half-width, $W/2$	$\tau = \sqrt{\kappa t}/(0.5W)$	As $\tau \to \infty$, $\Delta^+ \to 0.86$	At $\tau = 5.0$, $\Delta_2^+ = 5.5 \times 10^{-4}$
One-dimensional finite slab	Slab thickness, L	$\tau = \sqrt{\kappa t}/L$	For $\tau < 0.41$, $\Delta^+ = 0.125$	At $\tau = 1.1$, $\Delta_2^+ = 9.6 \times 10^{-4}$
GTPS/GTHS	Unit length, $L = 1$ m	$\tau = \sqrt{\kappa t}/L$	For all τ, $\Delta^+ = 0.125$	For all τ, $\Delta_2^+ = 0$ (cannot independently measure two parameters)
TPS	Sensor radius, R	$\tau = \sqrt{\kappa t}/R$	As $\tau \to \infty$, $\Delta^+ \to 1$	At $\tau = 1.85$, $\Delta_2^+ = 1.8 \times 10^{-3}$
CS where $H/R = 3$ and $H/W = 15$	Sensor half-width, $W/2$	$\tau = \sqrt{\kappa t}/(0.5W)$	At $\tau = 4.8$, $\Delta^+ = 0.35$	At $\tau = 1.83$, $\Delta_2^+ = 3.6 \times 10^{-4}$ and At $\tau = 17.2$, $\Delta_2^+ = 2.5 \times 10^{-3}$
GCS	Sample radius, R	$\tau = \sqrt{\kappa t}/R$	As $\tau \to \infty$, $\Delta^+ \to 0$ At $\tau = 0$, $\Delta^+ = 0.125$	At $\tau = 0.78$, $\Delta_2^+ = 5.7 \times 10^{-4}$

on other reasons, such as achieving a given level of confidence in the measured data through increasing the sample size.

The results for the one-dimensional finite slab are shown in Fig. 6. Note that the slab thickness, L, was used as the characteristic length scale in the definition of τ. For the single-parameter model, Δ^+ starts at a value of 0.125 and drops off sharply at $\tau = 0.41$. For the two-parameter model, a maximum Δ_2^+ of 9.6×10^{-4} occurs at $\tau = 1.1$. This result is similar to the GTHS/GTPS configuration with the exception that reflectance of the thermal wave at the finite boundary becomes important in the finite slab configuration at $\tau = 0.41$. This can be shown by comparing Fig. 5(c) with Fig. 6(c).

Of the four flat sensors investigated (THS, TPS, GTHS/GTPS, and 1D finite slab), the TPS sensor showed the largest values of Δ^+ and Δ_2^+ indicating highest sensitivity for both single- and two-parameter models.

The CS sensor results are shown in Fig. 7. The cylinder dimensions were the same as used in the model verification section: $R = 20$ mm, $H = 60$ mm, and $W = 4$ mm. This configuration could be described using two nondimensional length scales, $H/W = 15$ and $H/R = 3$. In the case of the CS sensor, there are several length scales from which to choose in the definition of τ. Here, τ was defined using the sensor half-width, $W/2$. Figure 7(c) shows a maximum Δ^+ of 0.35 occurring at $\tau = 4.8$; therefore, measurement sensitivity for thermal conductivity is highest for the CS sensor among all the sensors investigated in this work, including the TPS sensor. Figure 7(d) shows two local maxima: $\Delta_2^+ = 3.6 \times 10^{-4}$ at $\tau = 1.83$ and $\Delta_2^+ = 2.5 \times 10^{-3}$ at $\tau = 17.2$. The second peak in Δ_2^+ shows that the CS sensor will also have highest sensitivity for the two-parameter model of all the sensors investigated.

Finally, the GCS sensor results are shown in Fig. 8. The characteristic length scale was the sample radius, R. In Fig. 8(c), the optimization criterion for identifying thermal conductivity showed its maximum at early times, as τ approaches zero where Δ^+ approaches 0.125. A maximum was observed in the optimization criterion for the two-parameter model, where $\Delta_2^+ = 5.7 \times 10^{-4}$ at $\tau = 0.75$.

The results from this analysis are tabulated in Table 3, where the optimization criterion is given for each model in addition to the nondimensional times at which the maximum values occur. By comparing maximum values of Δ^+ and Δ_2^+, the TPS sensor showed best performance among the flat sensors and the CS sensor showed best performance among all the sensors considered. However, the time scales at which the maximum values of Δ^+ and Δ_2^+ occur must also be considered in the experimental design. For example, the CS sensor showed optimal performance at $\tau = 17.2$ for the two-parameter model while the TPS sensor showed optimal performance at $\tau = 1.85$. To maintain a given nondimensional time scale, τ, the experiment duration is increased for reduced diffusivity and/or increased sample length scale. For samples of low diffusivity and/or large length scales, $\tau = 17.2$ for the CS sensor may not be practical because the required experiment duration would be too long. The converse is also true, where the CS sensor may be more practical for samples of high diffusivity and/or smaller length scale.

Sensor Optimization for Cylindrical Configurations

In the previous section, the performance of various sensor configurations was quantified using Δ^+ for single-parameter estimates of λ and using Δ_2^+ for two-parameter estimates of λ and $\rho \cdot C_p$. In the present section, geometrical variations of the CS sensor are considered. Unlike the other sensor configurations considered in this paper (THS, 1D finite slab, GTHS/GTPS, and TPS), there are multiple length scales to consider with the CS sensor configuration. Specifically, the portion of heated area on the curved surface of the sample ($r = R$) is varied to determine the effect on optimization criteria.

As with previous analyses, the sample being considered is representative of stainless steel, where $\lambda = 16$ W/(m K) and $\kappa = 4.44$ mm^2/s. The applied heat flux is $q'' = 1000$ W/m^2. The sample radius and sensor width are held constant at $R = 20$ mm and $W = 4$ mm, respectively. The height of the sample is varied to represent four different sensor configurations, as shown in Fig. 9. Note that there is a perfectly insulated boundary condition at the ends of the cylindrical sample ($z = -H/2$ and $z = H/2$), which implies symmetry about these two planes. The CS sensor configuration is modeled as a single strip sensor on a single cylindrical sample, where $H \gg W$. The SCS sensor, on the other hand, is modeled as multiple parallel strips on the cylindrical sample where H is still greater than W but their ratio H/W is on the order of 1. Therefore, by keeping R and W constant, adjusting the height parameter in the CS model allows a transition between the CS and SCS configurations. In this analysis, the CS configuration has $H = 60$ mm such that $H/W = 15$. Two SCS configurations were considered, $H = 16$ mm ($H/W = 4$) and $H = 8$ mm ($H/W = 2$). The GCS configuration is described as the configuration where $H/W = 1$. In this manner, by moving from CS to SCS to GCS, the portion of heated area on the sample radius is systematically increased.

Figure 10(a) shows the optimization criterion, Δ^+, for single-parameter estimation of λ, and Fig. 10(b) shows the optimization criterion, Δ_2^+, for the estimation of λ and $\rho \cdot C_p$ using a two-parameter model. Note that the sample radius, R, is used in the definition of τ, to be consistent between reporting different configurations. In contrast, previous plots used the sensor width, W, for reporting CS sensor data. For the single-parameter model, Fig. 10(a) shows that decreasing the sample height results in decreasing maximum values of Δ^+. Another way to interpret this data is that by reducing the distance between adjacent strips on a cylindrical specimen, the measurement sensitivity will decrease. In the limit when there is no unheated area, $H/W = 1$, the GCS sensor configuration shows the lowest performance of the sensors considered. Additionally, the optimal experiment duration is reduced as the sensor strips are moved closer together. Figure

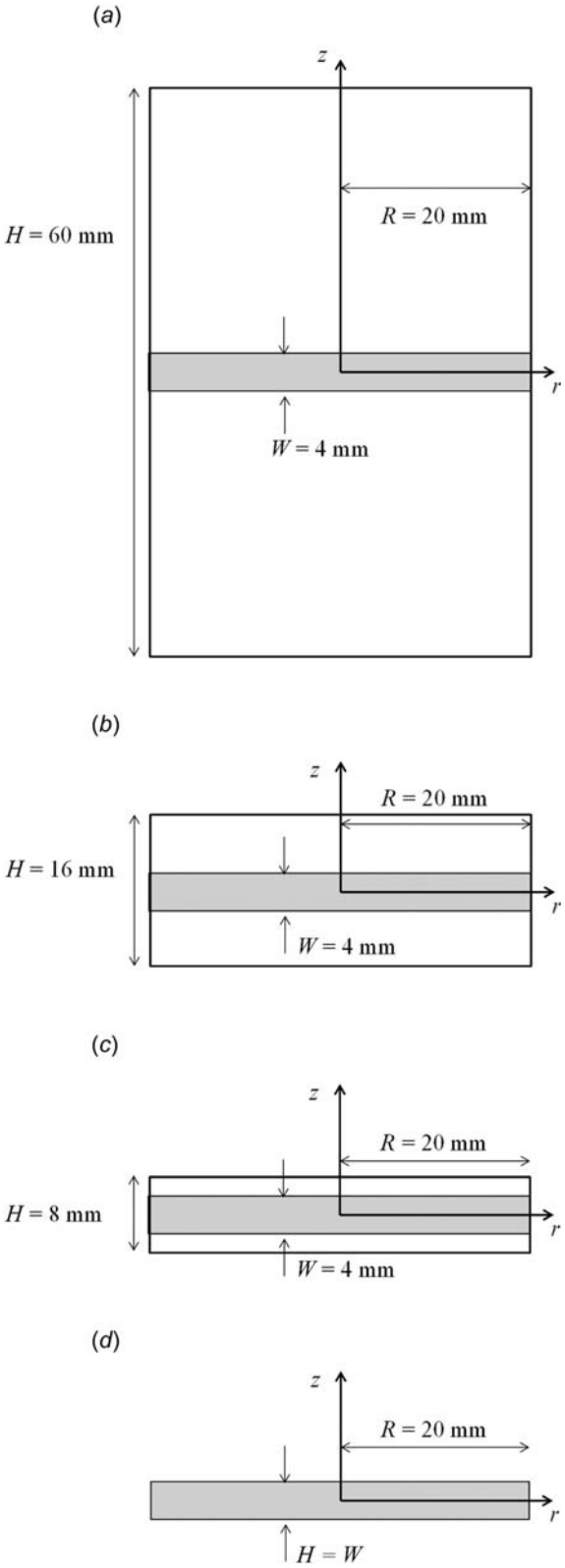

Fig. 9 Comparison of CS, SCS, and GCS sensors, showing the progression of increasing the portion of heated area (shaded). CS sensor with $H/W = 15$ (*a*), SCS_1 with $H/W = 4$ (*b*), SCS_2 with $H/W = 2$ (*c*), and GCS with $H/W = 1$ (*d*).

10(*b*) shows similar results for the optimization criterion, Δ_2^+, for estimation of λ and $\rho \cdot C_p$. Reducing separation distance between adjacent strips has the effect of reducing the maximum value of Δ_2^+ and reducing the time scale at which the maximum value of Δ_2^+ occurs.

One interesting implication of Fig. 10 is in the design of experiments for different materials or different size samples. For test samples of high thermal diffusivity or small length scale, it may be practical to carry out the experiment to the optimal time scale for the CS configuration, $\tau = 1.7$ as shown in Fig. 10(*b*). This would provide highest sensitivity for measuring both k and $\rho \cdot C_p$ of a cylindrical test sample. As the sample thermal diffusivity is reduced and/or length scale is increased, the experiment duration must be increased to maintain the nondimensional time scale, τ. In such circumstances, the experiment duration may be reduced by changing the sensor geometry. The GCS configuration, for example, reaches a maximum sensitivity at $\tau = 0.8$ in Fig. 10(*b*). Extending this concept to very low diffusivity samples or very large length scales, the time scale may be further reduced to $\tau = 0.19$ by making use of the local maximum in the CS sensitivity curve in Fig. 10(*b*). Although this local maximum has reduced measurement sensitivity compared to the global maximum at $\tau = 1.7$, the reduced experiment duration may be of greater importance, depending on the objectives of the experiment.

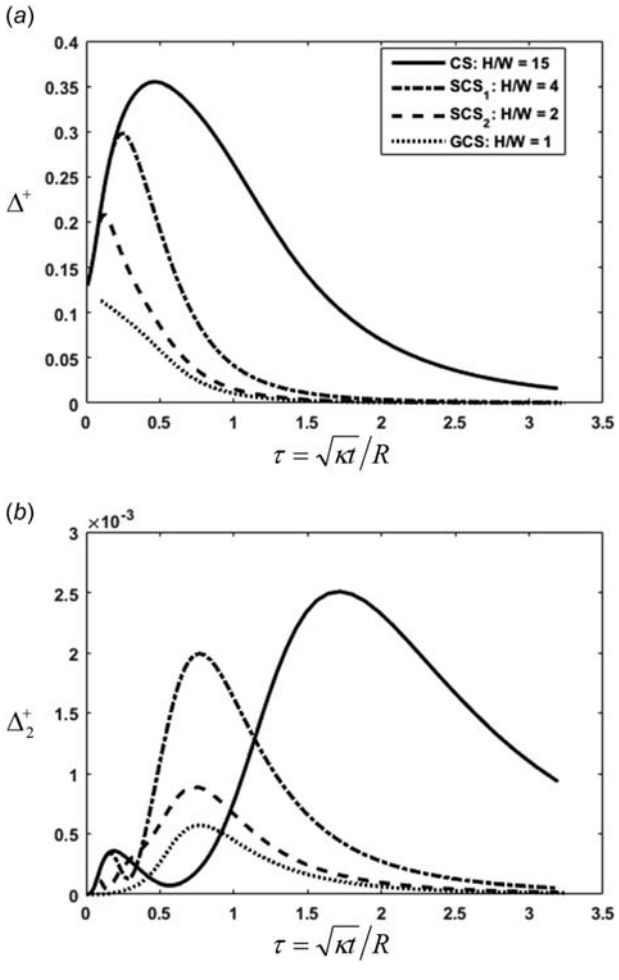

Fig. 10 Effect of separation distance between adjacent heater strips using the CS/SCS sensor. Decreasing separation distance results in reduced sensitivity to λ (*a*) as well as reduced sensitivity to simultaneous estimation of λ and $\rho \cdot C_p$ (*b*). (*a*) Single-parameter model and (*b*) two-parameter model.

Conclusions

Parameter estimation theory has been applied to characterize the performance of several new transient source based thermal property measurement approaches for cylindrical surfaces, and to compare against well-established sensor configurations for interrogation based on flat surfaces. The optimization criteria for both single- and two-parameter models are calculated and compared among the various sensors. Among the flat sensors, the TPS sensor shows the highest measurement sensitivity. However, the CS sensor showed the highest measurements sensitivity of all the configurations considered.

Furthermore, variations on the CS sensor are investigated, including the SCS and the GCS. Although these alternate configurations do not improve measurement sensitivity, the optimal time scale of the experiment may be reduced or the optimal length scale may be increased by increasing the ratio of heated to unheated area on the sample. The experimenter is, therefore, presented with a family of sensors to apply to cylindrical surfaces which provide tradeoffs in model performance versus experiment duration or length scale. The results from this paper are expected to facilitate the application of the transient source method to cylindrical geometries.

Acknowledgment

This work was funded under the Naval Innovative Science and Engineering (NISE) program as well as ONR Grant Nos. N00014-11-1-0659 and N00014-12-1-0594. This material is partly based upon work supported by CAREER Award No. CBET-1554183 from the National Science Foundation.

Nomenclature

- C_p = specific heat capacity
- $\mathbf{C}_{ij}^{+}$ = cumulative sensitivity coefficient matrix
- CS = cylindrical strip sensor
- GCS = guarded cylindrical strip sensor
- GTHS = guarded transient hot strip sensor
- GTPS = guarded transient plane source sensor
- H = height of cylindrical test sample
- L = length scale; thickness of 1D finite slab
- p = number of parameters to identify
- q'' = heat flux
- r = position along r-axis
- R = electrical resistance; radius
- s = Laplace transform variable
- SCS = spiral cylindrical strip sensor
- t = time
- T = temperature
- THS = transient hot source sensor
- TPS = transient plane source sensor
- W = width of sensor strip
- x = position along x-axis
- $\mathbf{X}_i^{+}$ = sensitivity coefficient vector
- y = position along y-axis
- z = position along z-axis

Greek Symbols

- β = thermal parameter of interest
- Δ^{+} = D-optimality criterion, single-parameter model
- Δ_2^{+} = D-optimality criterion, two-parameter model
- θ = temperature rise
- $\bar{\theta}$ = spatially averaged sensor temperature rise
- $\tilde{\theta}$ = Laplace-transformed average sensor temperature
- κ = thermal diffusivity
- λ = thermal conductivity
- ρ = density
- τ = nondimensional time
- ϕ = angular position

References

[1] Gustafsson, S., 1991, "Device for Measuring Thermal Properties of a Test Substance—The Transient Plane Source (TPS) Method," U.S. Patent No. 5,044,767.

[2] Gustafsson, S., Karawacki, E., and Khan, M. N., 1979, "Transient Hot-Strip Method for Simultaneously Measuring Thermal Conductivity and Thermal Diffusivity of Solids and Fluids," J. Phys. D: Appl. Phys., **12**(9), p. 1411.

[3] Gustafsson, S., and Karawacki, E. N., 1983, "Transient Hot-Strip Probe for Measuring Thermal Properties of Insulating Solids and Liquids," Rev. Sci. Instrum., **54**(6), pp. 744–747.

[4] Gustafsson, S., 1991, "Transient Plane Source Techniques for Thermal Conductivity and Thermal Diffusivity Measurements of Solid Materials," Rev. Sci. Instrum., **62**(3), pp. 797–804.

[5] Mathis, N., 1996, "Measurements of Thermal Conductivity Anisotropy in Polymer Materials," Ph.D. dissertation, University of New Brunswick, Fredericton, NB.

[6] Emmanuel, M., Zhao, C., Yu, B., Vinnik, D., and Rendell, C., 2014, "Method and Apparatus for Monitoring Materials," U.S. Patent No. 2014/0369379 A1.

[7] Bohac, V., Gustavsson, M., Kubicar, L., and Gustafsson, S., 2000, "Parameter Estimations for Measurements of Thermal Transport Properties With the Hot Disk Thermal Constants Analyzer," Rev. Sci. Instrum., **71**(6), pp. 2452–2455.

[8] Drake, S. J., Wetz, D. A., Ostanek, J. K., Miller, S. P., Heinzel, J. M., and Jain, A., 2014, "Measurement of Anisotropic Thermophysical Properties of Cylindrical Li-Ion Cells," J. Power Sources, **252**, pp. 298–304.

[9] Carslaw, H. S., and Jaeger, J. C., 1959, *Conduction of Heat in Solids*, Oxford University Press, London, UK.

[10] de Hoog, F. R., Knight, J. H., and Stokes, A. N., 1982, "An Improved Method for Numerical Inversion of Laplace Transforms," SIAM J. Sci. Stat. Comput., **3**(3), pp. 357–366.

[11] Beck, J. V., and Arnold, K. J., 1977, *Parameter Estimation in Engineering and Science*, Wiley, New York, NY.